


A Novel Deployable Open Ends Support Reflector

Dr. Muhsin J. Jweeg^{*}  Dr. Adnan D. Mohammed^{**}
Dr. Nabil N. Swadi^{**}

Received on:10/11/2006

Accepted on:6/9/2007

Abstract

This paper presents an improved deployable reflector concept for an Earth observation mission that requires a low-cost L-band Synthetic Aperture Radar (SAR) satellite. The required reflector shape is an offset parabolic cylinder with an arc length of 7.888 m and a width of 3.2 m. A novel **hollow solid** structural concept is proposed that comprises curved surfaces formed from thin sheets of carbon-fiber-reinforced-plastic (**CFRP**) connected by flexible hinges along the edges. This proposed structure has very high stiffness-to-weight-ratio, because of its thin-walled box-type construction. A preliminary design of the full-scale structure in deployed configuration, which has an estimated mass 22.5 kg and 18.665 kg and fundamental natural frequency of 0.72 Hz and 0.64 Hz before and after the optimization analysis respectively, is presented in the paper. This is 3.5 to 4.2 times lighter than the traditional reflector structure, made from lightweight curved panels with self-locking hinges. A detailed study of a quarter-scale technology demonstrator made of 0.6mm thick thermoplastic (nylon), including design, manufacture and testing is also presented.

SAR
3.2 7.888
CFRP
0.64 0.72 18.665 22.5
4.2 3.5
0.6

NOMENCLATURE

| | |
|--|---|
| a | = focal length |
| $d(x)$ | = perpendicular distance from the cord line to the parabola |
| E_1, E_2 | = lamina Young's moduli |
| F | = reflector performance |
| G_{12} | = lamina shear modulus |
| L | = length of window cutout |
| R_{\min} | = Minimum bend radius of the composite sheet |
| $s(x)$ | = arc length of the parabola |
| T | = sheet thickness |
| th | = thickness of the beam tube |
| u_x, u_y, u_z | = displacement in x, y, z direction |
| W | = width of window cutout |
| $\varepsilon_L^{(-)}, \varepsilon_L^{(+)}$ | = longitudinal ultimate strains in compression and tension |
| $\varepsilon_T^{(-)}, \varepsilon_T^{(+)}$ | = transverse ultimate strains in compression and tension |
| ε_{LT}^f | = ultimate shear strain |
| δ_{ex} | = root mean square error |
| ρ | = mass density |

INTRODUCTION

New structural concepts for large deployable spacecraft are currently being developed to meet the needs of low cost missions using small satellite. General requirements include the ability to deploy large surfaces in space or orbit (flat or curved, depending on the mission) using structure of low mass and sufficient stiffness. It is also required that these structures stow in a compact volume and deploy reliably to the correct shape.

Figure 1, represents the flight configuration of traditional reflector. This reflector includes four lightweight, curved sandwich panels, connected by self-locking hinges [1]. **EADS** Astrium estimated the mass of this structure at 79 kg [2]. The required reflector shape is an offset parabolic cylinder with an arc-length of 7.9 m and width of 3.2 m.

This paper presents an alternative design, much lighter concept. The idea is

to form a hollow solid from thin, curved sheets of **CFRP**, connected by flexible hinges along the edges, which forms continuous reflective surface that has the required shape for the reflector.

This structure has good stiffness-to-mass-ratio, because of its thin-walled box-type construction.

A brief outline of the paper is as follows. The section Structural Concept explains the proposed approach and the section Cutting Pattern derives the cutting pattern for the four sheets that make the reflector. Then, the sections Design for Folding and Design of Reflector Structure outline the stages of the design process of this novel structure, including the design of the preliminary design of a full-scale flight reflector and quarter-scale groundwork reflector made of **CFRP**, and the analytical estimation of the minimum bend radius of the sheet material. Detailed finite-element analyses of the static, modal, buckling optimization, behaviors of both quarter-scale and full-scale reflectors are obtained. The construction, surface accuracy, stiffness to weight ratio, and focal distance of the quarter-scale plastic model are presented.

STRUCTURAL CONCEPT

Consider a flat sheet A with curved edge, connected to another flat B, as shown in Figure 2(a). If sheet A is rotated through 90°, both sheets become curved, as shown in Figure 2(b).

Now consider the hollow solid support structure shown in Figure 3, made by connecting two pairs of identical flat sheets. Sheets A and A', which are identical, are connected to sheets B and B', which are also identical. The shape of the curved edges is identical in all four sheets. The shape of the hollow solid is defined by the cutting pattern of the sheets. The folding configuration shown in Figure 3(a), is obtained by moving the broken lines in

the middle of sheets A and A' shown in Figure 3(c) inward.

Once the hollow solid support structure has been flattened (stage 1 of the folding process) it can then be folded longitudinally (stage 2 of the folding process) as an accordion, or a coil, as shown in Figure 3(b).

A reflective surface of cylindrical shape can be formed by replacing sheet B with a rectangular sheet, see Figure 4.

The explanation of how to determine the edge profile of sheet A is as follows. Figure 5(a) shows two curved surfaces, A and B, that intersect along the curve OEA. Surface B can be created by considering the two-dimensional curve $z=d(x)$, and by translating it to along a generator segment, e.g. BC, parallel to y-axis. It is to be noted that in Figure 5(a) a general point on $z=d(x)$ is point B; also note that the x-axis starts at the origin O and passes through the end point A of the curve. Finally, note that all points on BC have the same arc-length distance s from the y-axis, and same distance d from the xy plane.

Let F and D be the projections of B and E onto the xy plane, clearly

$$BF=DE=d \quad (1)$$

Now if one considers the flattening of the surface B onto the xy-plane, without moving its edge along y-axis, then during this process BC moves in the x and z directions, while remaining parallel to the y-axis. The distance d of E above the xy-plane becomes zero.

It is clear that the locus of points E on the surface B defining the curved profile of surface A, and hence the curve along which the two surfaces are attached. It will be assumed that the generator BC is perpendicular to the surface A in the deployed configuration. In addition, it will also be assumed that the two surfaces are joined to each other at the general point E and there is no relative

motion of the join points when the surfaces are flattened.

The following conditions apply

- Condition 1: The arc-length of OE, measured on the surface B is equal to the arc-length of OE measured on the surface A.
- Condition 2: When the surface are flattened, both points B and D move towards point F, and so B and D coincide when the surfaces are flattened, Figure 5(b). Hence it follows that

$$BE=DE=d \quad (2)$$

From the above, a three-dimensional cylindrical surface (surface B) can be defined by a two-dimensional curve $z=d(x)$. First it is required to determine the arc-length, $s(x)$, along the curve and then to determine the edge profile of surface A given by $d(x)$. Note that $d(x)$ also defines the curve along which surface A is to be connected to surface B. It is to be noted that, from Equation 2, both sheets have the same singly curved shape in the deployed configuration.

CUTTING PATTERN

In this section, the cutting pattern for the sheets of the reflector structure has been worked out to provide the required focal length, aperture, and offset distance.

The required parabolic profile for the reflective surface (RF) is shown in Figure 6. The cutting pattern of the flat sheets requires the arc-length $s(x)$ and the perpendicular distance from the cord line to the parabola $d(x)$ to be calculated.

From the equation of a parabola with vertex at origin and that of a general curved line, the arc-length $s(x)$ and $d(x)$ are calculated in the following form

$$s(x) = \sqrt{x(x+a)} - \sqrt{x_o(x_o+a)} + \frac{a}{2} \ln \left(\frac{2x+a+2\sqrt{x(x+a)}}{2x_o+a+2\sqrt{x_o(x_o+a)}} \right) \quad (3) \text{ and}$$

$$d(x) = \sqrt{\frac{(xa_1 + a_o - k\sqrt{x})^2}{1 + a_1^2}} \quad (4)$$

where $a_o = (y_o x_f - x_o y_f) / (x_f - x_o)$, a_1 is the slope of the chord line, and a is the focal length.

The cutting pattern for the flat sheets, defined by $s(x)$ and $d(x)$ in Equations 3 and 4, is shown in Figure 7.

Two more parameters are needed to completely determine the cutting pattern for the open ends support reflector. These parameters are the height (2H) and width (2W) of the support. Their magnitudes are determined by thinking about the size of the packaged structure and by optimization the performance of the reflector in the deployed configuration.

DESIGN FOR FOLDING

As it stated above, the reflector structure is constructed from thin sheets of **CFRP**.

This section presents the analysis of those elements of the reflector body that need to elastically deformed in order to allow folding of the reflector.

Connections

All connections must be strong enough to transfer the loads from one surface to another, and flexible enough to allow folding and unfolding of the reflector. The connections must prevent the relative translation between matching points on two lines of separate sheets, but allow the sheets to rotate. Figure 8 presents two types of connections used for this purposes. They have been made with adhesive tape in order to provide a uniform stress distribution across the two sheets in connection.

Minimum bend radius R_{min}

To ensure that no material failure occurs during folding of the reflector structure, R_{min} of the **CFRP** sheets was estimated theoretically.

The maximum strain criterion assumes that failure of a laminated

composite occurs when the in-plane strains along the principal material directions exceed the ultimate strains of the material, [3]

$$\begin{aligned} -\varepsilon_L^{(-)} &< \varepsilon_1 < \varepsilon_L^{(+)} \\ -\varepsilon_T^{(-)} &< \varepsilon_2 < \varepsilon_T^{(+)} \\ |\gamma_{12}| &< \varepsilon_{LT} \end{aligned} \quad (5)$$

where $\varepsilon_L^{(-)}$ and $\varepsilon_L^{(+)}$ are the longitudinal ultimate strains in compression and tension; $\varepsilon_T^{(-)}$ and $\varepsilon_T^{(+)}$ are the transverse ultimate strains in compression and tension; and ε_{LT} is the ultimate shear strain.

Consider a flat, symmetric, balanced laminated plate, initially unstressed. A large curvature is imposed along the x-axis and, since the in-plane stiffness of the plate prevents it from stretching, the plate deforms into approximately cylindrical surface, i.e. the transverse radius of curvature in the fold region is zero. Clearly, since

$\kappa_x \neq 0, \varepsilon_x^o = \varepsilon_y^o = \gamma_{xy}^o = \kappa_y = \kappa_{xy} = 0$, the in-plane strains along the principal material directions become

$$\begin{Bmatrix} \varepsilon_1 \\ \varepsilon_2 \\ \gamma_{12}/2 \end{Bmatrix}_j = \begin{bmatrix} zm^2 \\ zn^2 \\ -zmn \end{bmatrix} \begin{Bmatrix} \kappa_x \\ \kappa_y \\ \kappa_{xy} \end{Bmatrix} \quad (6)$$

where m and n are the cosine and sine of the ply angle for lamina j.

In an isotropic plate, and also in the case of unidirectional composite plate bent along its principal material direction, the maximum strain occurs on the outer edges of the plates, hence at $z = \pm t/2$. Of course, the peak bending strains are compared with the ultimate strains for fibers. However, numerous experiments on thin laminates made from woven **CFRP** composites [4, 5] have shown that these laminates are able to survive peak bending strains that are

much larger than those obtained from the above approach. Therefore, here it will be assumed that a woven lamina in bending fails when the strain at the center of the outermost yarn reaches the ultimate value:

$$\begin{aligned}\varepsilon_x &= \pm z \kappa_x \\ \varepsilon_y &= \gamma_{xy} = 0\end{aligned}\quad (7)$$

where z is the distance of the center of the outermost fibre from the mid-plane. Therefore, minimum radius of curvature can be obtained from the ultimate strain ε_{\max} (which is equal to the smaller of $\varepsilon_L^{(-)}$ or $\varepsilon_L^{(+)}$, in the case of laminated composite):

$$R_{\min} = \frac{1}{\kappa_x} = \frac{z}{\varepsilon_{\max}} \quad (8)$$

The minimum bend radii (R_{\min}) were estimated and are listed in Table 1 for the composite plates made of woven **T300** carbon in **LTM45** epoxy resin of the material properties: $E_1 = E_2 = 70$ GPa, $G_{12} = 5$ GPa, $\nu_{12} = 0.05$, $\rho = 1560$ kg/m³, $V_f = 60$ %, $\varepsilon_L^{(-)} = 1$ %, $\varepsilon_L^{(+)} = 1$ %, and for assumed ultimate shear strain $\varepsilon_{LT}^f = 3.6$ % [5]

Table 1: Minimum bend radius of **T300/LT45** woven laminates.

| Lay up | L mm | W mm | T mm | κ_x | R_{\min} mm |
|-------------------------------------|---------|---------|---------|------------|------------------|
| 0 | 85 | 20 | 0.125 | 0.32 | 3.1 |
| 0/0 | 85 | 20 | 0.25 | 0.10 | 9.3 |
| 0/45/0 | 85 | 20 | 0.30 | 0.08 | 12.5 |
| 45/0/45 | 85 | 20 | 0.30 | 0.16 | 6.2 |
| (0/45 ₂ /0) _s | 85 | 20 | 0.30 | 0.07 | 14.0 |

Note that from Table 1, the use of angle plies on the outer surfaces of the plate significantly decreases the estimated minimum bend radius.

Sizing of Cutouts in Side walls R_{\min}

Cutouts are required to reduce the maximum strain in the region where a hinge line crosses another hinge line in the same sheet of material. It is desirable for these cutouts to be as small as possible, to reduce the loss of stiffness of the reflector body. Stress concentrations must be minimized near the corners of these cutouts by introducing rounded corners [6]. In this paper, only cutouts for Z-folding (accordion) were investigated in detail.

The width W of the cut-out has to be such that the sidewall can be bent 180° along the line H_1H_1 , as shown in Figure 9. To prevent materials failure, it is required that

$$W \geq \pi R_{\min} \quad (9)$$

The length L of the cutout is determined by taking into account fold about the line H_2H_2 in Figure 10, in flattened reflector structure. Assuming that all the surfaces of the reflector structure have the same thickness and material properties, and consequently the same R_{\min} , the length L of the cutout can be estimated from

$$L \geq 2\pi R_{\min} + \pi T \quad (10)$$

Note that, if the radius of curvature is assumed to be R_{\min} everywhere, the inner part of the sidewall would hold up with the outer part; but this can be eliminated by considering a fold with a non-uniform radius.

DESIGN OF OPEN ENDS SUPPORT REFLECTOR

Two versions of the open ends support reflector were designed. The first version is a full-scale structure designed for the flight-loading environment. The second version is a quarter-scale structure that can be tested in the laboratory, under 1g loading conditions. The focal length of this demonstrator is quarter, and it is made from sheets of CFRP with the

same wall thickness that would be used for the first version (full-scale) reflector.

Structural Analysis of Reflector

The two above versions of reflector were modeled with the ANSYS finite element program [7]. The aim of the analysis was to study the static, dynamic, and buckling response of the reflector, in the deployed configuration. The optimal weight of the full-scale reflector has been obtained using the optimization design analysis.

The four concave surfaces that make up the reflector were separately defined. Then, the structure was assembled by connecting the sidewalls along their edges to the RF surface and to the back surface.

In the ANSYS model it was assumed that the four sides of the first quarter of the RF surface have momentless connections, i.e. $u_x=u_y=u_z=0$.

All surfaces are made of woven carbon T300/LM45 composite with eight layers $(0/45_2/0)_s$, with uniform thickness and average material properties defined in section Minimum Bend Radius above. An inertial loading of 0.02 m/s^2 along the focal axis, i.e. the x-axis in Figure 6, was applied.

An initial analysis showed that stiffening the ends and RF surface of the reflector with thin walled tube stiffeners and thin rectangular ribs respectively, increased the fundamental natural frequency and decreased the maximum displacement of the structure significantly.

The tubes ($r_1=5\text{mm}$, $r_2=7\text{mm}$, $th = 1\text{mm}$) and ribs ($10\text{mm} \times 0.125\text{mm} \times 3.2\text{m}$) are made in the same material as that the structure made from.

Different designs were compared by means of a multi-objective optimization performance criterion. This criterion was based on reducing the mass, increasing the deployed stiffness of the structure, and increasing the safety margin against buckling failure as

follows:

$$F = K_1 \frac{WT_{ref}}{WT} + K_2 \frac{USUM_{ref}}{USUM} + K_3 \frac{f_o}{f_{oref}} + K_4 \frac{\xi_{3ref}}{\xi_3} + K_5 \frac{B_{Lref}}{B_L} + K_6 \frac{B_{Gref}}{B_G} \quad (11)$$

where

K_i = weighting factor

WT= total mass of the reflector (kg)

USUM= maximum displacement (mm)

ϕ_3 = margin against material failure given by the Tsai-Wu criterion

B_L =margin against local buckling (%)

B_G =margin against global buckling (%)

This analysis showed that the best option had a wall thickness of 0.3mm for the sidewalls and back surface and of 0.25mm for the RF surface, and symmetric sidewalls and back surface with $2H=2W=2m$. Figure 11 shows the loading and boundary conditions of full-scale demonstrator.

The optimal reflector had an overall mass of 22.5kg, maximum displacement of 0.0219mm, first natural frequency of 0.72Hz, and eigenvalue of the first buckling mode of 121.2, before optimization process, see Figures 12 to 14

Non-symmetric sidewalls, leading to a tapered design of the reflector support structure, were also investigated.

When the optimization process has been carried out, the new optimal reflector (for no stiffening) had an overall mass 18.66kg, and first natural frequency of 0.64Hz, as shown in Figure 15.

A detailed analysis of the quarter-scale QS demonstrator was carried out. The finite element model of the demonstrator is shown in Figure 16, where the vector g denotes the direction of gravity. Note that each sidewall has three cutouts (windows) whose dimensions are (form Equations 9

and 10 for R_{min} of 14mm and T of 0.3mm with a certain margins) 180mm long and 50mm wide.

The same material properties were used for this demonstrator but for (0/45/0) laminate, and uniform thickness of 0.3mm for all surfaces.

A contour plot of the maximum displacement magnitudes due to gravity loading, assuming that the structure is suspended horizontally through four points as shown in Figure 16, obtained from a linear static analysis are shown in Figure 17(a). Note that the maximum displacement magnitude, 1.479mm, occurs at the edges of the sidewalls at the tip end of the demonstrator. The margins against material failure, evaluated using the Tsai-Wu failure criterion, and against global buckling, were found to be huge. They were 58.65e-03 and 90.23e-02 respectively. The first natural frequency was about 16.57Hz.

Additional stiffening of the sidewalls was provided by attaching tape springs to the vertical edges of all the cutouts. The total mass of the demonstrator was estimated at 1.552kg. The maximum displacement magnitude is reduced to about 76.4 %. The margin against material failure, margin against global buckling and first natural frequency are increased to about 88.5 %, 68.5 % and 18.5 % respectively.

Figure 17(b) shows the contour plot of the displacement magnitude after adding the tape springs to sidewalls.

Figure 18 illustrates the first vibration mode of the QS demonstrator before and after adding the tape springs.

TESTING OF QS MODEL

Due to unavailability of the CFRP composite sheets, the thermoplastic (Nylon) sheets of 0.6 mm thick are used instead. The plastic sheets and the rectangular stiffeners made from plywood of 15mm x 3mm were prepared. The tape springs were made by

cutting suitable lengths of steel tape measure. 28mm high cup-and cone spacers made of lightwood were made for the sidewalls, on either side of each line H_1H_1 . All connections were made with special adhesive tape, see Figure 19. The structure was assembled and its total mass was 2.55kg. Further details on the parts and assembly process are available in [8].

Measurements of surface accuracy and stiffness to weight ratios were taken in the deployed configuration. The stiffness and surface accuracy were measured after first deployment.

Measurement of Surface Accuracy of QS Plastic Model

A manual procedure was used to measure the surface accuracy of the RF surface of the QS plastic demonstrator for only the bottom edge. 840 circular equally spaced targets were attached to the RF surface (40 target points attached to the bottom edge of the RF surface). The measurements were carried out after packaging and deploying the structure.

The equation of the best-fit parabola, in a coordinate system in which X and Y are parallel to x and y , respectively, and X_o and Y_o are the measured coordinate of the vertex of the parabola, is

$$X = \left(X_o + \frac{Y_o^2}{4a^*} \right) - \frac{Y_o}{2a^*} Y + \frac{1}{4a^*} Y^2 \quad (12)$$

where a^* is the focal length of the best-fit parabola.

For n target points that are equally spaced on the RF surface, the root mean square (RMS) error in the axial direction X , with respect to the best-fit parabola, is calculated from [9]

$$\delta_{ex} = \sqrt{\frac{\sum (\hat{X}_i - X_i)^2}{n}} \quad (13)$$

where \hat{X}_i is the axial coordinate of a general target point and X_i is the

corresponding axial coordinate of the best-fit parabola.

Figure 20 shows the comparison of the distortion or best fit and design parabola for QS plastic model after deploying. The best-fit focal length $a^*=0.78384\text{m}$, which is closes to focal length of the design parabola, $a=0.77225\text{m}$; this 1.5% difference may be due to highly reflector's distortions under gravity. The RMS error of this model was calculated to be 4.1718mm. this rather disappointing value is due to errors during manufacturing and manual measurements. To reduce this error, the distance between the stiffeners of the RF surface must be minimized, and glued perfectly perpendicular to the long edges of RF surface.

Measurements of Stiffness

Displacements measurements of the tip end of the structure were carried out in the deployed configuration. These measurements were taken using a dial gauge of 0.01mm accuracy.

Static loads in the out-of-plane, transverse, and longitudinal directions were applied to the tip end of the reflector structure, by means of string and pulley system. The displacements in the direction of the load were measured in each test, and then a linear best-fit relationship was obtained, in order to estimate the stiffness and then the stiffness to weight ration of the structure for each load case. Figures 21 to 23 show a comparison between the measured and the estimated values from an ANSYS linear-elastic static analysis. The ANSYS model is stiffer in all cases, by 33.2% in out-of-plane direction, by 32.4% in the transverse direction, and by 49% in the longitudinal direction.

Obviously, some modification of the model (e.g. by measuring the actual elastic properties of the sheets, plywood, and tape springs) would be desirable. From Figures 21 to 23, it is clear that the

reflector is stiffer in the longitudinal direction.

PACKAGING OF THE QS PLASTIC DEMONSTRATOR

Packaging consists in flattening the structure and then introducing three transverse folds that allow it to fold into an accordion. The folding sequence of the QS plastic model is shown in Figure 24.

Flattening the reflector involves bending the sidewalls through 180°. The process needs to be carefully controlled, to prevent damaging the reflector structure. First, the model is placed on the wood mold, with the RF surface facing down and the back surface facing up. Plugs fit snugly inside the hollow solid are placed inside the reflector to prevent it from collapsing.

Next, flattening of the reflector is initiated by pulling the sidewalls inwards with a pair of wooden poles placed outside the reflector, between the sets of cup and cone spacers. When the poles are loaded, the plugs are slowly pulled out to allow the back surface to arrive down. Once the back surface stopped coming down under its weight, weights are added on top of the back surface to bring it down, and then the demonstrator became substantially flattened (stage 1 of folding).

Longitudinal folding is much simpler than flattening. First, the two ends are rotated through 180°, making sure that the RF surface ends up on the outside, and then the middle fold is introduced, this time placing the RF surface on the inside, (stage 2 of folding).

The stowed volume was measured equal to 0.05127 m^3 .

COCLUSIONS

1. A new concept of large deployable reflectors for SAR applications has been presented.
2. At full scale, it has been estimated that the proposed

approach leads to a structure weighing 22.54kg and 18.66kg, before and after optimization process respectively, which is 3.5 and 4.2 times lighter than the traditional reflector structure.

3. The QS plastic model has achieved a surface accuracy of 4.1718mm RMS, typical mass 0.83kg/m², focal length of 1.5% difference, packaging density of 0.05127m³ i.e. 1/15th of deployed volume, and a typical deployed frequency of 6.338Hz.

References

- [1]PELLEGRINO, S., and WATT, A. M. "Tape Spring Rolling Hinges" Proceedings of 36th Aerospace Mechanisms Symposium, Glenn Research Center, 15-17 May 2002.
- [2]HOWARD, P. "Technical Note: Satellite Definition for Land Hazards Mission" WP 4200A, 3991-04660-RPZ, EADS-Astrium, 2001.
- [3]GIBSON, R. F. "PRINCIPLES OF COMPOSITE MATERIAL MECHANICS" McGraw-Hill Book co., Singapore, 1994.
- [4]YEE, J. C. H. and PELLEGRINO, S. "Folding of Woven Composite Structures" Composites/ Part A, Vol. 36, No.2, 2005.
- [5]GERNGROSS, T. "Folding of Thin-Walled Composite Structures" Technical University of Munich, Munich TUM-MW 65/ 0331-SA, 2003.
- [6]NIU, M. C. "AIR FRAME STRUCUTRAL DESIGN" Connilit Press Ltd, California, USA, 1988.
- [7]KONHKI, P. C. " ANSYS: User's Manual, Release 9" SAS.IP Inc, 2004.
- [8]NABIL, N. S. "Shape Optimization of Paraboloidal Surface reflectors under static and Dynamic loadings" PhD Thesis, University of Technology, Baghdad, 2006.
- [9]LEVY, R. "Structural Engineering of Microwave Antennas" The Institute of Electrical and Electronics Engineers, New York, 1996.

913 914 915 916 894 895 896
897 898 899 900

903 904 905 906 910 911 912

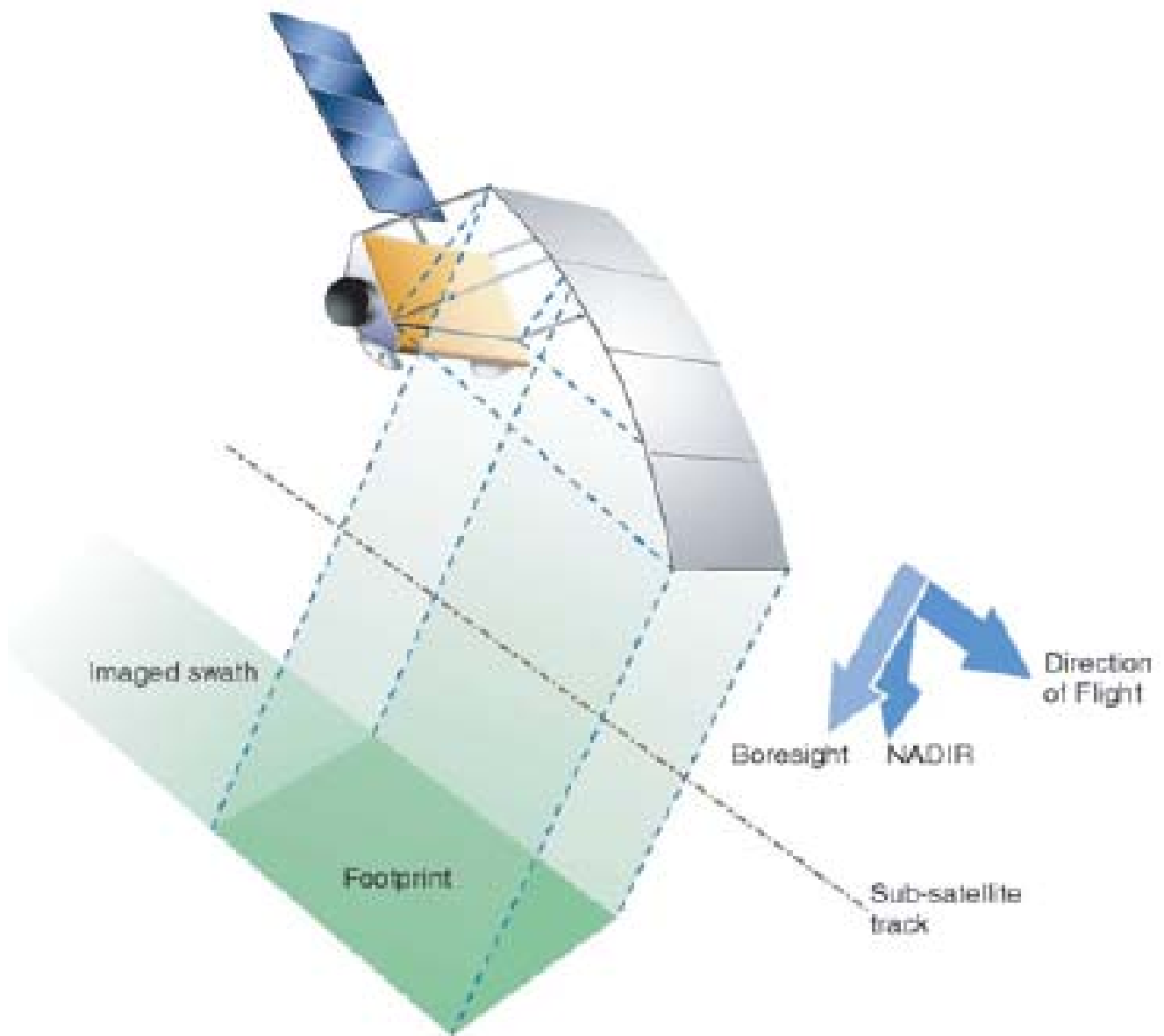
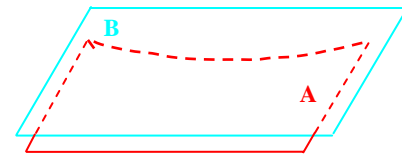
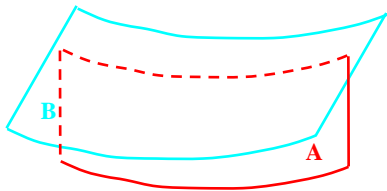


Figure 1: Traditional reflector, flight configuration.

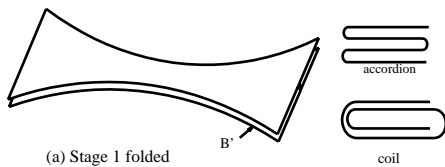


(a) Flat (curved

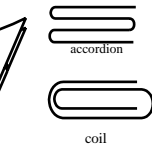


(b) Deformed (curved

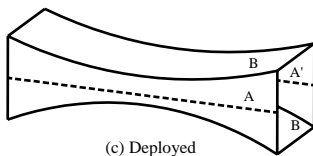
Figure 2: Use of a shaped sheet A to form sheet B.



(a) Stage 1 folded



(b) Stage 2 folded



(c) Deployed

Figure 3: Hollow solid supporting structure.

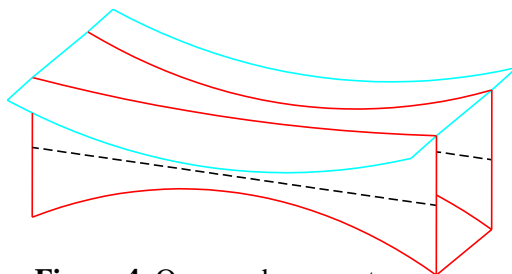
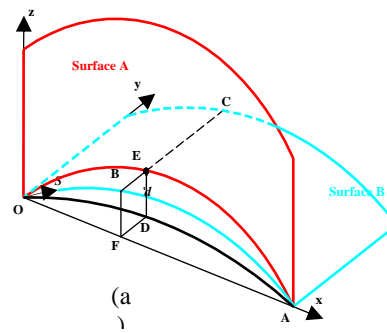
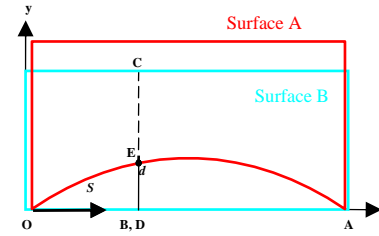


Figure 4: Open ends support reflector in deployed configuration.



(a)



(b)

Figure 5: Required edge profile of sheet A to form singly curved surface.

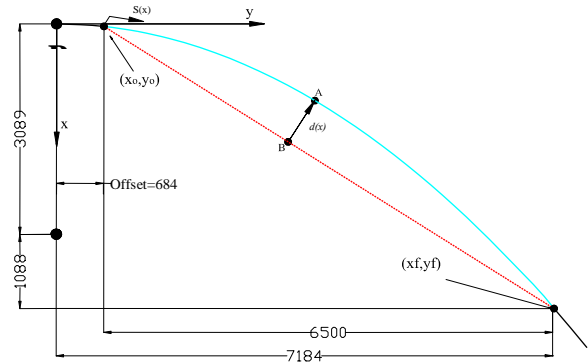
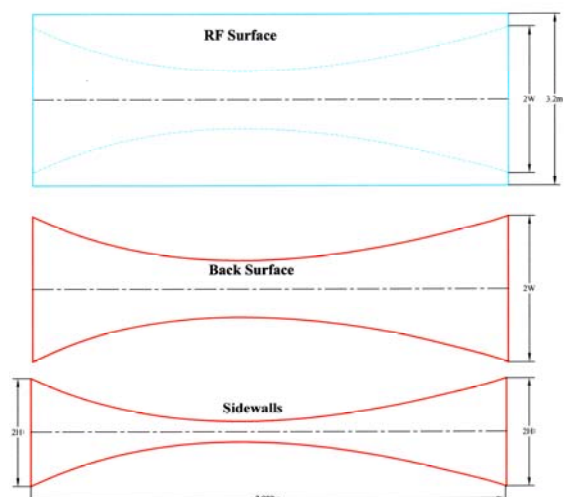


Figure 6: Profile of RF surface (dimensions in mm)

Figure 7: Cutting pattern for the open ends support reflector.



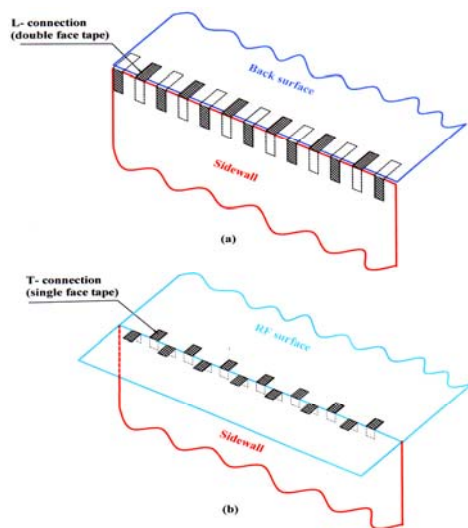


Figure 8: Types of connection.

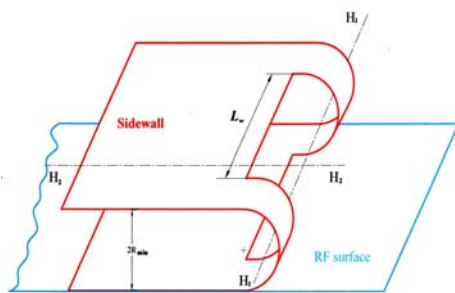


Figure 9: Folding of side wall about line H_1H_1 .

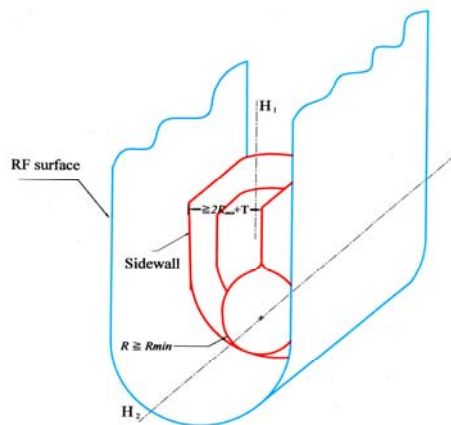


Figure 10: Folding of RF surface around folded sidewall.

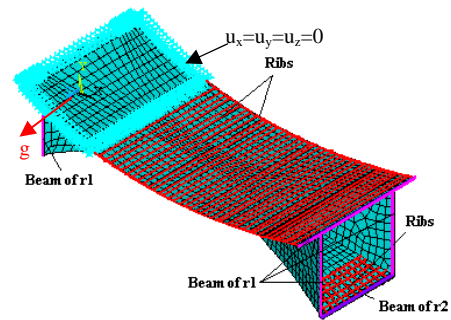


Figure 11: Loading and BCs of full-scale demonstrator.

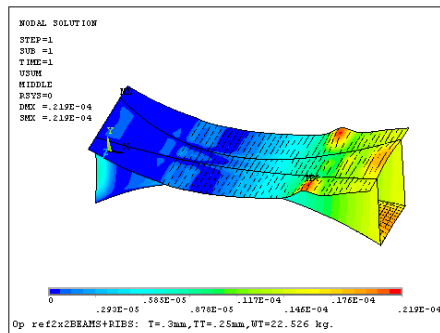


Figure 12: Contours of maximum displacement magnitudes (m).

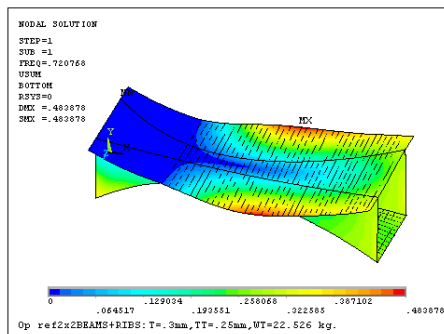


Figure 13: First vibration mode, frequency= 0.72Hz.

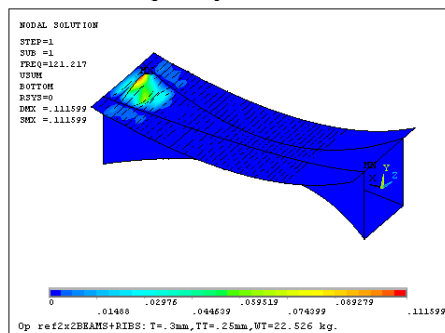


Figure 14: First buckling mode, eigenvalue = 121.2.

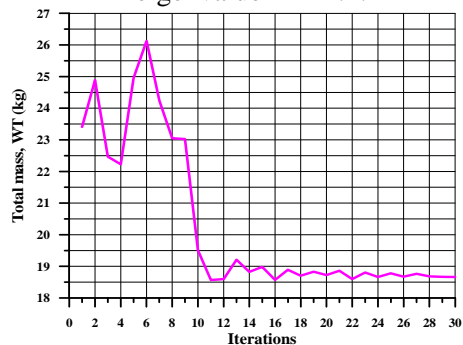


Figure 15: Evaluation of overall mass during the optimization process.

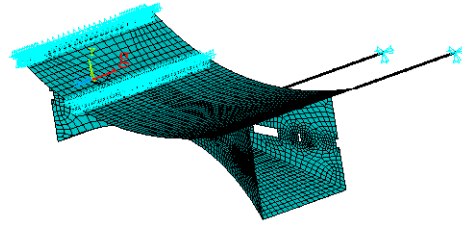
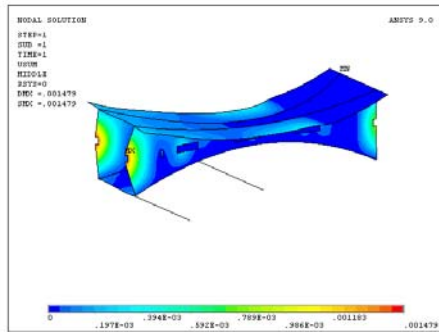
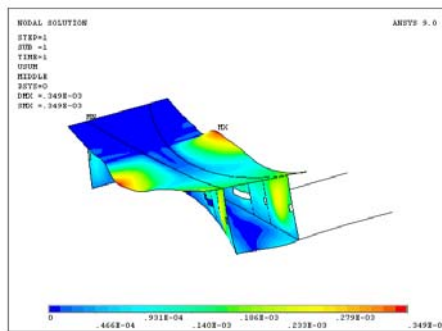


Figure 16: BCs and loading of QS demonstrator.

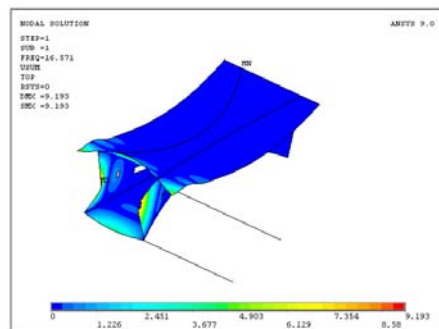


(a) Without tape springs

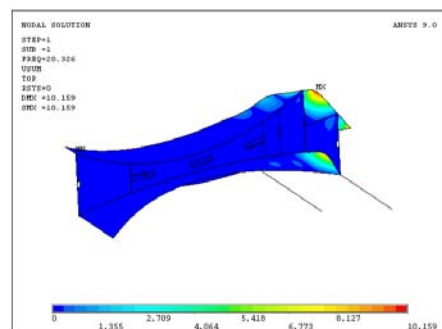


(b) With tape springs

Figure 17: Contours of maximum displacement magnitude (m), of QS model.



(a) Without tape springs (freq.=16.57Hz)



(b) With tape springs (freq.=20.32Hz)

Figure 18: First vibration mode of QS model.

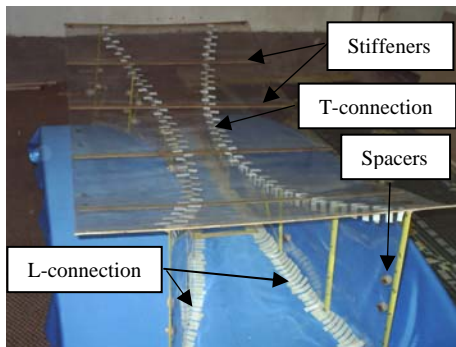


Figure 19: QS plastic model open ends reflector.

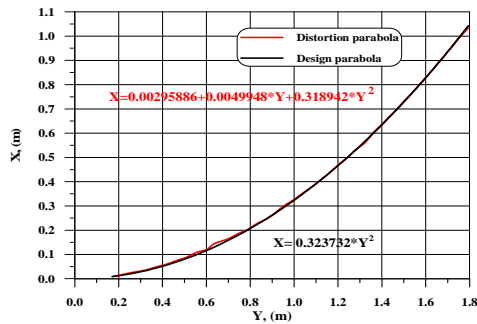


Figure 20: Comparison of the best-fit and design parabola for QS plastic model reflector.

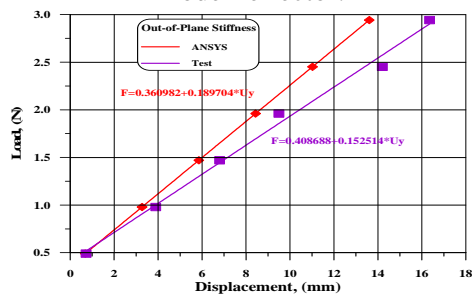


Figure 21: Comparison of out-of-plane stiffness.

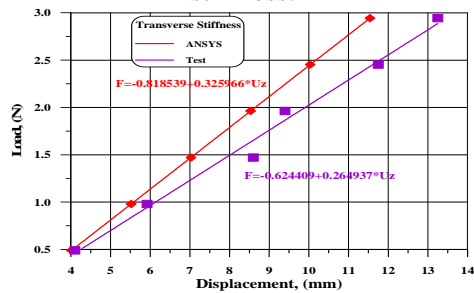


Figure 22: Comparison of transverse stiffness.

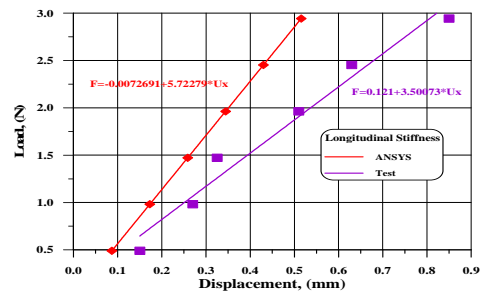
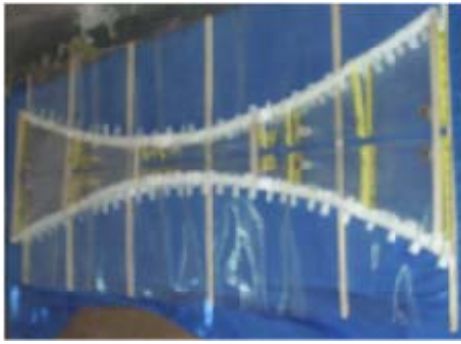
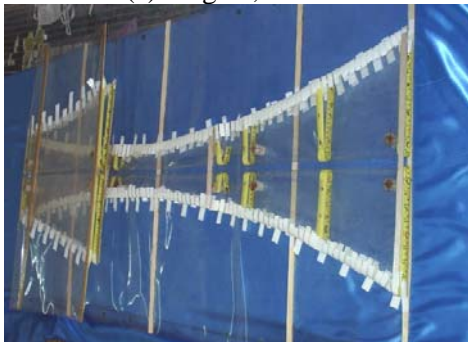


Figure 23: Comparison of longitudinal stiffness.



(a) Stage 1, flattened



(b) Step 1 of stage 2, folded.



(c) Step 2 of stage 2, folded.



(d) Step 3 of stage 2, folded.

Figure 24: Packaging sequence of QS plastic model.

Received on:10/11/2006

Accepted on:6/9/2007

Sizing of Cutouts in Side walls R_{min}